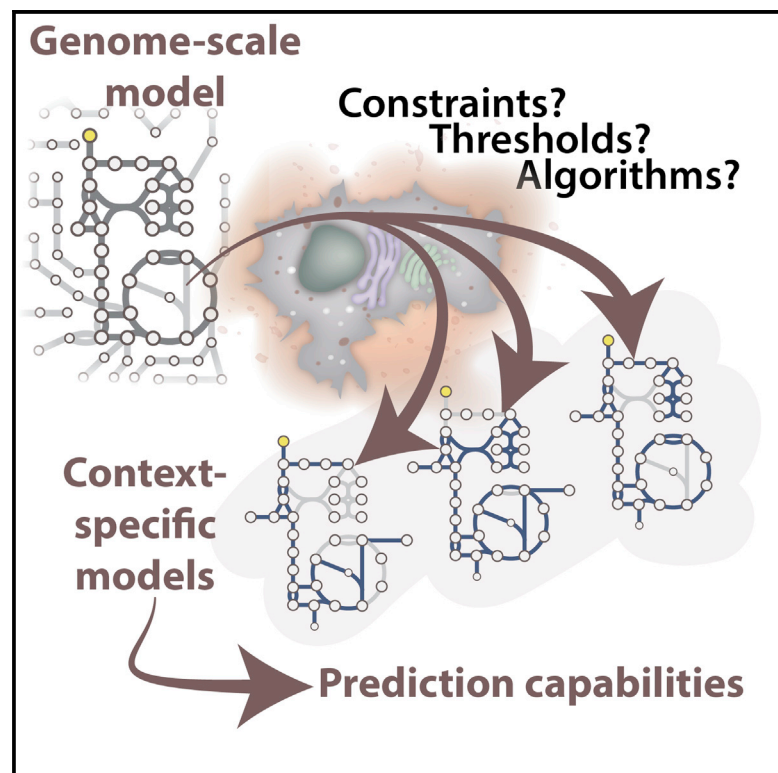


# Cell Systems

## A Systematic Evaluation of Methods for Tailoring Genome-Scale Metabolic Models

### Graphical Abstract



### Authors

Sjoerd Opdam, Anne Richelle,  
Benjamin Kellman, Shanzhong Li,  
Daniel C. Zielinski, Nathan E. Lewis

### Correspondence

nlewisres@ucsd.edu

### In Brief

This study presents a comparative analysis of hundreds of models built for four different cancer cell lines using several prominent model extraction algorithms. The evaluation provides insights into how their assumptions affect the prediction capabilities of context-specific models.

### Highlights

- Hundreds of models have been built for four cancer cell lines
- The performance of model extraction algorithms and parameter sets are evaluated
- Different parameters and algorithms yielded diverse models
- Extraction method most strongly affected accuracy of gene-essentiality predictions

# A Systematic Evaluation of Methods for Tailoring Genome-Scale Metabolic Models

Sjoerd Opdam,<sup>1,2,6</sup> Anne Richelle,<sup>2,3,6</sup> Benjamin Kellman,<sup>2,4</sup> Shanzhong Li,<sup>2,5</sup> Daniel C. Zielinski,<sup>2,5</sup> and Nathan E. Lewis<sup>2,3,4,7,\*</sup>

<sup>1</sup>Department of Biomedical Engineering, Computational Biology, Eindhoven University of Technology, 5612 AZ Eindhoven, the Netherlands

<sup>2</sup>Novo Nordisk Foundation Center for Biosustainability at UC San Diego

<sup>3</sup>Department of Pediatrics

University of California, San Diego, School of Medicine, La Jolla, CA 92093, USA

<sup>4</sup>Bioinformatics and Systems Biology Program, University of California, San Diego, La Jolla, CA 92093, USA

<sup>5</sup>Department of Bioengineering, University of California, San Diego, La Jolla, CA 92093, USA

<sup>6</sup>Co-first author

<sup>7</sup>Lead Contact

\*Correspondence: [nlewisres@ucsd.edu](mailto:nlewisres@ucsd.edu)

<http://dx.doi.org/10.1016/j.cels.2017.01.010>

## SUMMARY

Genome-scale models of metabolism can illuminate the molecular basis of cell phenotypes. Since some enzymes are only active in specific cell types, several algorithms use omics data to construct cell-line- and tissue-specific metabolic models from genome-scale models. However, these methods are often not rigorously benchmarked, and it is unclear how algorithm and parameter selection (e.g., gene expression thresholds, metabolic constraints) affects model content and predictive accuracy. To investigate this, we built hundreds of models of four different cancer cell lines using six algorithms, four gene expression thresholds, and three sets of metabolic constraints. Model content varied substantially across different parameter sets, but the algorithms generally increased accuracy in gene essentiality predictions. However, model extraction method choice had the largest impact on model accuracy. We further highlight how assumptions during model development influence model prediction accuracy. These insights will guide further development of context-specific models, thus more accurately resolving genotype-phenotype relationships.

## INTRODUCTION

Large-scale omics experiments are now standard in many biological studies, and many methods exist to interpret these data. One emerging approach uses genome-scale metabolic models (GEMs) as valuable systems biology platforms for model-guided data analysis of large omics datasets, since they provide cellular context to the data (Hyduke et al., 2013). Furthermore, they allow the integration of diverse omics data since they catalog all metabolic reactions in an organism, and the reactions

directly link metabolites to enzymes. They can further elucidate how changes in one component affect other pathways and cell phenotypes since these models connect genes to measurable cell phenotypes (e.g., growth, cell energetics, pathway fluxes, biosynthesis of cell components, byproduct secretion, etc.) (Lewis et al., 2012). Thus, these systems biology models can provide a mechanistic link from genotype to phenotype, leading to novel insights and guiding further experiments. For example, these models have helped identify antimicrobial and anti-cancer drug targets (Folger et al., 2011; Frezza et al., 2011; Ho Sui et al., 2012; Kim et al., 2014; Lewis and Abdel-Haleem, 2013; Shen et al., 2010; Yizhak et al., 2015) and identify mechanisms underlying other diseases (Lewis et al., 2010; Martinoglu et al., 2014), among many other applications (Bordbar et al., 2014).

Recent algorithmic developments have claimed to allow researchers to build GEMs that more accurately capture the metabolism of individual tissues or cell types. Specifically, GEMs include all reactions in an organism, but not all enzymes are active in a given tissue or cell line (Uhlen et al., 2015). Therefore, algorithms have been developed to extract cell-line- or tissue-specific models (sometimes referred to more generally as context-specific models) that recapitulate the metabolism of specific cell types (Becker and Palsson, 2008; Wang et al., 2012; Zur et al., 2010). A context-specific model is a subset of the GEM, in which inactive reactions are removed. Reaction removal is determined by the algorithm used, gene expression levels, presence of proteins or metabolites, experimental data availability, literature knowledge, and/or predefined metabolic functions of the cell type that need to be maintained in the extracted model.

It is assumed that context-specific models better represent the actual metabolism of a cell or tissue. Initial procedures for testing context-specific models have been proposed (Pacheco et al., 2015), but the assumptions underlying the extraction methods have not been rigorously tested for mammalian models. Thus, here we evaluate the performance of several prominent model extraction algorithms, analyze the impact of their assumptions, and quantify the influence of key decisions that must be made when building cell-line- and tissue-specific

**Table 1. The MEMs Tested in This Study**

MEM	Description	Data Type and Usage	Handling Missing Expression Evidence (Orphan/Missing Data)	Requires Metabolic Objective
FASTCORE (Vlassis et al., 2014)	Define one set of core reactions that is guaranteed to be active in the extracted model and find the minimum number of reactions possible to support the core.	Any data type can be used to define the core reaction set.	removed if not necessary to support core reactions	no
GIMME (Becker and Palsson, 2008)	Minimize usage of low-expression reactions while keeping the objective (e.g., biomass) above a certain value. Does not favor inclusion of reactions not related to the objective.	Transcriptomic data are most straightforward to define low-expressed reactions and their respective weights.	does not explicitly favor removal or inclusion	yes
iMAT (Shlomi et al., 2008) (Zur et al., 2010)	Find the optimal trade-off between including high-expression reactions and removing low-expression reactions.	Any data type can be used to define high- and low-expression reactions.	does not explicitly favor removal or inclusion	no
INIT (Agren et al., 2012)	Find the optimal trade-off between including and removing reactions based on their given weights. If desired, accumulation of certain metabolites can be allowed or even forced.	Any data type can be used to define the weights. Assignment of weights based on the data can be done in multiple ways.	removal or inclusion determined by user-defined weights	no
MBA (Jerby et al., 2010)	Define high-confidence reactions to ensure activity in the extracted model. Medium confidence reactions are only kept when a certain parsimony trade-off is met. In random order, prune other reactions and remove them if not required to support high- or medium-confidence reactions.	Any data type can be used to define the high- and medium confidence reactions.	removed if not necessary to support high- or medium confidence reactions	no
mCADRE (Wang et al., 2012)	Define a set of core reactions and prune all other reactions based on their expression, connectivity to core and confidence score. Remove reactions not necessary to support the core or defined functionalities. Core reactions are only removed if supported by a certain number of zero-expression reactions.	Transcriptomic data are most straightforward to determine the order of pruning, the core reactions, and the zero-expression reactions.	removed if not necessary to support core reactions	no

models. We do this through the comparative analysis of hundreds of models, extracted for four cancer cell lines (A375, HL60, K562, and KBM7). Models were built after constraining the genome-scale model of human metabolism using three sets of constraints based on exometabolomics data. Six algorithms (MBA, mCADRE, GIMME, INIT, iMAT, and FastCore) were used to build extracted models based on four gene expression thresholds to specify the active genes in each cell line from RNA sequencing (RNA-seq). We analyzed the content of the models and tested their ability to predict gene essentiality, as measured using CRISPR-Cas9-mediated loss-of-function screens. We further test the ability of algorithms to discover the metabolic functions of individual cell types, based solely on omics data. Through this effort we elucidate a hierarchy of three key decisions (i.e., algorithm used, gene expression threshold, and input model constraint) that significantly affect the accuracy of cell-line- and tissue-specific models, and also provide guidelines for the future development of more accurate algorithms.

## RESULTS

Model extraction methods (MEMs) employ diverse algorithms to extract cell-line- or tissue-specific models from a GEM (Table 1). The MEMs we have considered can be categorized into three families: “GIMME-like” (i.e., GIMME), “iMAT-like” (i.e., iMAT and INIT), and “MBA-like” (i.e., MBA, FASTCORE, and mCADRE), as proposed previously (Robaina Estévez and Nikoloski, 2014). The GIMME-like family minimizes flux through reactions associated with low gene expression. The iMAT-like family finds an optimal trade-off between removing reactions associated with low gene expression, and keeping reactions whose genes/enzymes are highly expressed. In the MBA-like family, the algorithms use sets of core reactions that should be retained and active, while removing other reactions if possible. Different MEMs were often explicitly designed to integrate specific omics data types (e.g., transcriptomics, proteomics, metabolomics, etc.), but can easily and intuitively be adapted to use other types, such as RNA-seq and exometabolomics,

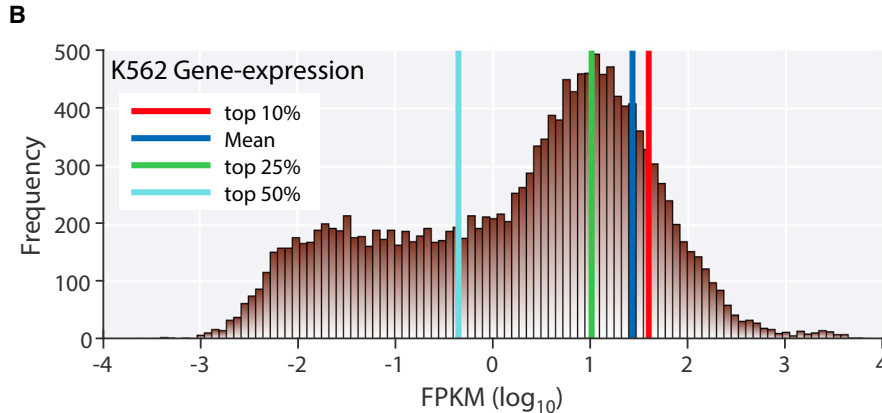
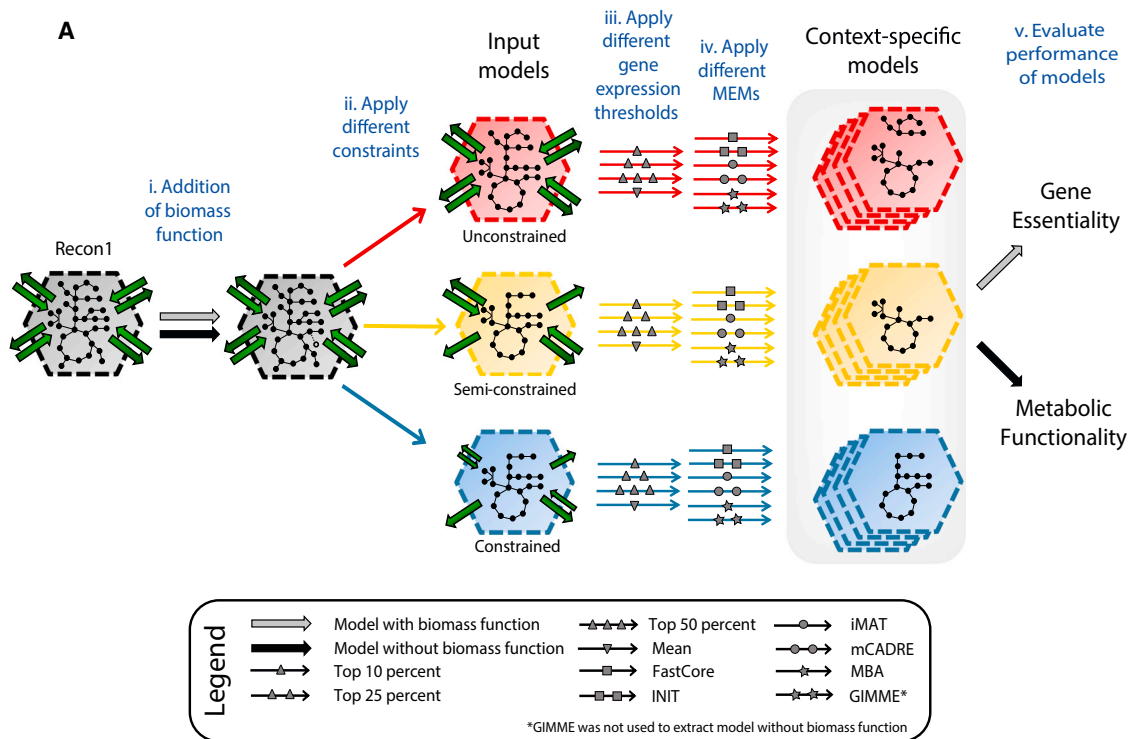


**Figure 1. Hundreds of Cancer Cell-Line-Specific Models Were Constructed to Evaluate Different Approaches to Model Extraction**

(A) For four cell lines, 528 cell-line-specific models were built from three input models with different metabolite uptake/secretion constraint sets, six different MEMs, and four expression thresholds.

(B) Most algorithms require users to define which genes are “expressed,” so we defined four thresholds, as shown here for the K562 cell line.

which we use in this study. See [STAR Methods](#) for detailed descriptions of the MEMs tested in this study, parameter selection, and details on small simplifications to MEMs to ensure consistency of comparisons (e.g., use of a single threshold for iMAT).

### Models are Extracted for Four Cancer Cell Lines

When extracting a cell-line-specific model, several decisions must be made. Three most salient are (1) how to constrain the uptake and secretion fluxes in the model prior to model extraction, (2) which MEM algorithm to use for extraction, and (3) the threshold used to call a gene “expressed.” In this study, we analyzed how these decisions affect the model content, predic-

tive capacity for gene essentiality, and ability to capture metabolic functionality (Figure 1A) for four different cancer cell lines (i.e., A375 melanoma cells and HL60, KBM7, and K562 leukemia cells). We built models from Recon 1 (Duarte et al., 2007). Models were built both with and without the addition of a biomass function, consisting of 56 metabolites required for growth (Table S1). To ensure the robustness of the results of this study, we further varied the setup parameters. For example, qualitatively similar results were obtained with a recently published update to the human GEM, Recon 2.2 (Swainston et al., 2016). Moderate variations of the biomass function composition and non-growth-associated maintenance factor also resulted in similar results (see [STAR](#)

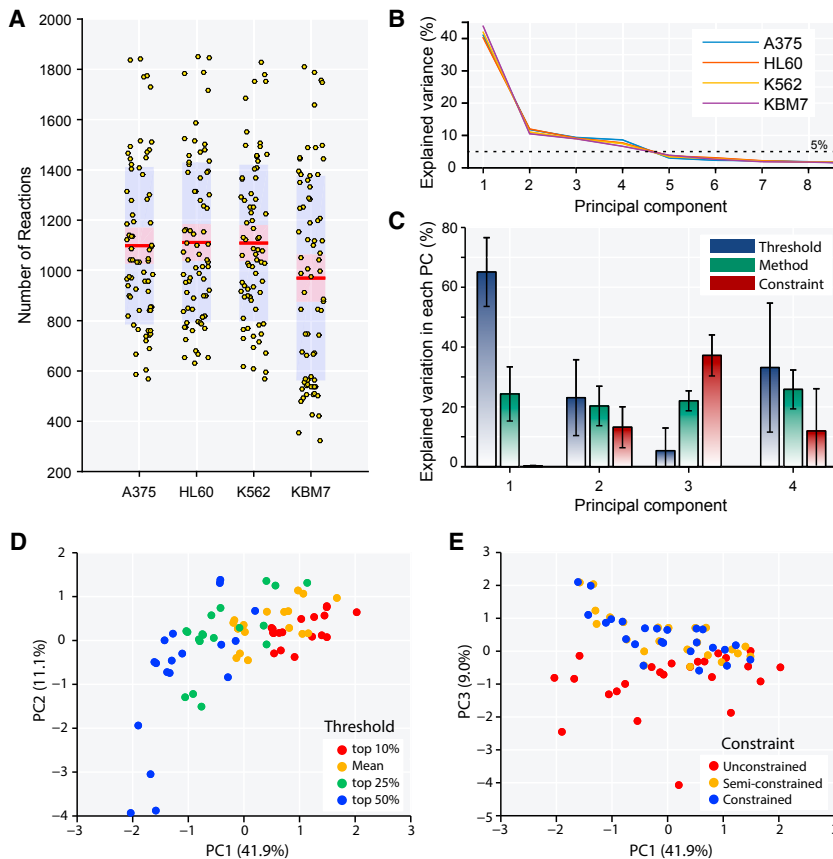


**Figure 2. Decisions in Cell-Line-Specific Model Extraction Considerably Affect Model Content**

(A) Seventy-two different combinations of algorithms and reasonable parameter sets led to a large diversity of cell-line-specific models of different sizes.

(B) The first four principal components (PCs) explain most of the variance in reaction content of the models.

(C) The gene expression threshold contributes the most to the first PC for all cell lines and the model constraint selection dominates the third PC. The MEM contributes significantly to each PC. Error bars indicate SE across the four cell lines.

(D and E) The influence of expression threshold selection is clear in the first PC for the K562 cell line (D), while the model scores of the third principal component for the K562 cell line is clearly influenced by the constraint type that was used to extract the models (E).

Methods and Figures S1 and S2). Finally, some MEMs can produce multiple models that differ in a small number of reactions (e.g., iMAT and MBA) and these alternate models provided similar results in this study (see STAR Methods and Figures S3 and S4).

To allow the comparison of different constraints, we developed three different input models for the two different setups of Recon 1 (i.e., with and without a biomass function). We call the three input models the “unconstrained,” “semi-constrained,” and “constrained” models (Figure 1A), and these three input models differed in if and how exometabolomic data were used to constrain exchange reactions (metabolite uptake and secretion reactions) in Recon 1. Specifically, the unconstrained model has all exchange reactions open, so it can take up or excrete all metabolites allowed by the reconstruction. For the semi-constrained models, exchange reactions are qualitatively constrained to a specific directionality based on if the metabolites were taken up or secreted in exometabolomic datasets (Jain et al., 2012). The constrained models have quantitatively constrained uptake and secretion rates for the measured metabolites. Quantitative values were based on changes in metabolite levels in the media of a panel of cancer cell lines (Jain et al., 2012). In each input model, biomass was constrained to the experimentally measured growth rate of the cell lines (see STAR Methods for more detail).

We built cell-line-specific models using RNA-seq data (Bürckstümmer et al., 2013; Di Ruscio et al., 2013; Pawlikowski et al., 2013; Zhang et al., 2015) to specify active genes in each cell line. Active genes are identified by many algorithms based on a quantitative threshold of expression. To cover a range of

representative thresholds, four gene expression thresholds were defined to specify which genes are “expressed” in the models: top 10%, mean, top 25%, and top 50% (Figures 1B and S5).

To test the predictive capacity of the models against experimental gene essentiality, we used CRISPR-Cas9 loss-of-function screens for each cell line (Shalem et al., 2014; Wang et al., 2014, 2015). We also tested the capacity of each extracted model to recover a panel of metabolic functionalities defined based on the biomass function.

In summary, 528 models were built from Recon 1 (288 and 240 models with and without the biomass function, respectively) using three types of constraints, six MEMs (Table 1), and four expression thresholds for four different cancer cell lines. Thus, these provided a controlled set of models to assess the influence of experimental data, algorithm, and related parameter settings on the content and performance of the extracted model.

### Model Content Is Most Affected by Threshold Selection

Decisions regarding gene expression threshold, algorithm choice, and the exchange constraints affect the content of our cell-line-specific models. Specifically, the extracted cell-line-specific models varied considerably in size from <600 reactions to >1,800 reactions (Figure 2A). To assess the impact of each decision on model content, we conducted a principal component analysis (PCA) of the reactions in all models for each cell line. The first principal component explains >40% of the overall variance in reaction content for each cell line (Figure 2B). In all four cell lines, the choice of gene expression threshold provides the most significant contribution to the variation in the first principal component ( $p < 1.5 \times 10^{-13}$ ; Figures 2C, 2D, and S6).

MEM selection provides a moderate contribution to the explained variation in each principal component (Figure 2C). Meanwhile, the type of uptake/secretion constraint only significantly contributes to the third principal component ( $p < 1.3 \times 10^{-6}$ ; Figures 2C, 2E, and S6), which accounts for ~10% of the variance in

model content. These results are consistent across cell lines and indicate that the content of a cell-line-specific model is most heavily affected by the choice of gene expression threshold, followed by the choice of MEM and constraints placed on metabolite uptake and secretion.

### Model Extraction Improves Gene-Essentiality Prediction

GEMs contain the genetic basis of cell growth and maintenance. Thus, microbial GEMs have been particularly successful in predicting gene knockout phenotypes (Covert et al., 2004; Edwards and Palsson, 2000). Further work demonstrated that some gene knockdown phenotypes can be predicted for human cell lines (Folger et al., 2011; Gatto et al., 2015). However, it is unclear how accurately human cell-line-specific models predict essential genes, and how sensitive the accuracy is to the different decisions made for model extraction.

To address this, we compared model-predicted gene essentiality with data from genome-wide CRISPR-Cas9 loss-of-function screens for the four cancer cell lines (Shalem et al., 2014; Wang et al., 2014, 2015). In these screens, essential genes are identified by quantifying single guide RNA (sgRNA) abundance for each knockout before and after growth selection. A large decrease in sgRNA abundance indicates a strong impairment of growth. We systematically deleted each gene in each of the 288 models with the biomass function, and then used flux balance analysis (Schellenberger et al., 2011) to test models for normal or impaired growth. We then tested if the sgRNA abundances decreased significantly for the model-predicted essential genes (one-tailed Wilcoxon rank-sum test). The p value from this test quantifies accuracy, with a lower p value indicating a better agreement between model prediction and experimental data (see STAR Methods).

During model extraction, reactions are removed from the input model, and through the process, genes that are initially non-essential in the GEM can become essential in the cell-line-specific model. Different combinations of MEMs, thresholds, and uptake constraints lead to different sets of predicted essential genes for the extracted model. However, almost all cell-line-specific models more accurately predict essential genes than the input GEMs (Figure 3A). Furthermore, the different decisions in model construction affect the accuracy of gene-essentiality predictions (Figure S7). First, more stringent gene expression thresholds lead to more accurate gene-essentiality predictions (Figure 3B). Second, constrained models are more accurate than unconstrained models (Figure 3C). Third, the MEMs differ in accuracy at predicting gene essentiality (Figure 3D). Combinations of different parameters and MEMs can be analyzed to find models with more accurate gene-essentiality predictions (Figures 3E, 3F, and S8). Across all cell lines, we found that gene-essentiality predictions of INIT, MBA, and mCADRE are the most accurate, especially when using the most stringent gene expression thresholds (top 10% and mean). However, iMAT and INIT have a larger spread in p values than MBA and mCADRE (Figure 3D), since accuracy decreases substantially for when using the unconstrained (iMAT and INIT) and semi-constrained (iMAT) setups for model extraction.

To identify which decision has the greatest impact on the ability to accurately predict gene essentiality with cell-line-specific

models, we quantified the proportion of the variance in the accuracy scores explained by each decision (Figure 3G). Surprisingly, MEM choice had the greatest impact on the accuracy, in contrast to gene expression threshold, which had the largest impact on whether reactions were included in a model (Figure 2C).

### Metabolic Functionalities Are Not Always Maintained after Model Extraction

Many human tissues have unique metabolic functions they accomplish. However, it can be difficult to define all tissue-specific metabolic functions a priori in an unbiased fashion, since they are often poorly defined for a given tissue. Can extracted models capture these metabolic functions in an unbiased fashion when tissue- or cell-line-specific data are used to build the models? To answer this, we tested the extent to which the MEMs can recapitulate a panel of essential metabolic functions for the four cell lines studied here.

Not all metabolic functions are known, but we defined 56 metabolic functions that are essential for cancer cell growth, based on the biomass function (Figure 4A). This includes the synthesis of non-secreted metabolites (e.g., ATP, carnitine, and glutathione). To this end, 240 models were built for the four cell lines using Recon 1 without a biomass function, along with the various gene thresholds, uptake constraints and MEMs in this study (except for GIMME, since it requires the prior definition of metabolic functions). We then tested if the 56 functions were predicted to be included in each extracted model without a priori definition of these functionalities, and a “functionality score” was assigned to each model. The score represents the number of additional functionalities of a cell-line-specific model exhibited beyond the number for the 99<sup>th</sup> quantile of comparable models of the same size generated from randomized data (see STAR Methods).

Almost all cell-line-specific models achieve more metabolic functions than expected by random chance (Figure 4B). However, some important metabolic functions are inactivated in many individual models (Figure 4A). A PCA of the functionalities that were present or absent across the cell lines demonstrated that the gene expression threshold explained, on average, 51% of the variation in the first principal component, while the MEM choice explained 17% of the variation (Figure 4C). Constraint selection was the dominant decision in the second principal component, but only explained 19% of the variation. To understand why some functionalities are missed more often, we analyzed two cancer-relevant metabolites (phosphatidylinositol and tryptophan) that are not available in many of the models.

Phosphatidylinositol is a substrate of the phosphatidylinositol 3-kinase enzymes, which are over-active in many tumors and can drive tumor progression (Vivanco and Sawyers, 2002). Phosphatidylinositol exists in several different phosphorylated states, and the transitions between different states form a metabolic cycle (Figure 4E). Some reactions associated with the cycle, such as PI3P4K, are highly expressed and therefore are present in the cell-line-specific models. Since the reactions form a cycle, the steady-state assumption underlying GEMs allows the cycle to be included, even when the reaction supplying metabolites into this cycle, phosphatidylinositol synthase (CDIPT<sub>r</sub>), or upstream reactions are removed, as seen for 61% of the models

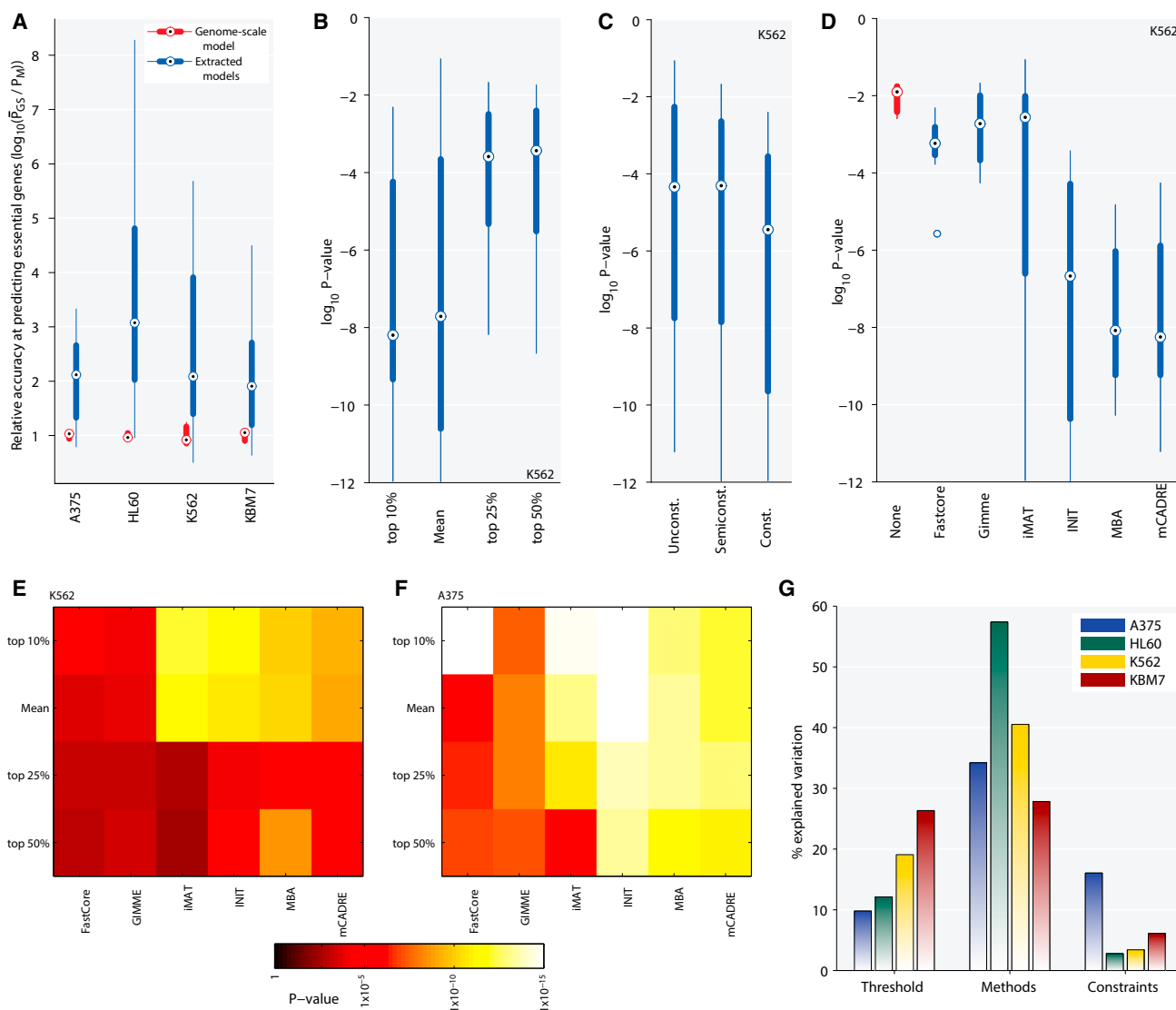


**Figure 3. Cell-Line-Specific Models Predict Gene Essentiality, but Accuracy Is Most Strongly Influenced by the MEM**

(A) We compared the accuracy of the unconstrained, semi-constrained, and constrained GEMs without MEM use (red) and after MEM use (blue). The relative accuracy is the  $\log_{10}$  of the average Wilcoxon p values of the GEMs ( $\bar{P}_{GS}$ ), divided by the p value ( $P_M$ ) for each genome-scale (red) or cell-line-specific model (blue). (B) More stringent threshold cutoffs resulted in more accurate gene-essentiality predictions, as shown for the K562 cell line. (C and D) Constrained models resulted in slightly more accurate gene-essentiality predictions in the K562 cell line (C), and the different MEMs demonstrated different levels of accuracy in predicting gene essentiality (D). (E and F) Combinations of different thresholds and algorithms result in more accurate models, as shown using the constrained input model for the K562 (E) and A375 (F) cell lines. (G) When all decisions are assessed, the selection of MEM contributes the most to the accuracy of the model-predicted gene essentiality.

(Figure 4D). This inhibits the net production of phosphatidylinositol by most cell-line-specific models (Figures 4D and 4E). Thus, even if a metabolite is present in a cell-line-specific model, the model may not be able to predict the physiological metabolic function of producing the metabolite due to “loops” resulting from the steady-state assumption of COBRA models (Noor et al., 2012).

Tryptophan consumption is also absent from many models, despite its critical role in facilitating escape from the immune response in progressive cancer (Prendergast, 2011). This is

achieved as tryptophan is converted to kynurenine (Lkynr) due to high activity of indoleamine-2,3-dioxygenase 1 and 2 (*IDO1* and *IDO2*) and tryptophan-2,3-dioxygenase (*TDO*). The models fail to predict tryptophan-associated functions because of multiple problems (Figure 4F). First, tryptophan is an essential amino acid, used for the synthesis of protein and several hormones and metabolites. Thus, it must be taken up from the medium. However, the confidence intervals on the exometabolomic data used in this study were so wide that their range of values include zero, and so even the constrained models are not forced to take



up tryptophan. Second, since tryptophan uptake can be zero, the pathways using tryptophan will only be activated if downstream reactions are associated with highly expressed genes that force their inclusion in the cell-line-specific model. Since many reactions in the tryptophan-consuming pathway show low gene expression, many MEMs remove the entire pathway. It is possible that high thresholds fail to include important genes if they show high catalytic rates or function at low metabolic rates. Third, some algorithms will eliminate reactions even when they are associated with highly expressed genes if they are involved in a pathway with more reactions with low gene expression (e.g., iMAT, mCADRE, etc.). Fourth, the GPRs for the tryptophan 2,3-dioxygenase reaction (TROP2) in Recon 1 are missing for two of the three enzymes that catalyze it. These include the IDO1 and IDO2 isozymes that are highly expressed in some cancers (Prendergast, 2011). Therefore, the tryptophan 2,3-dioxygenase reaction (TRPO2) is not always assigned to a gene expression level and the MEMs favor its removal.

As shown here, many combinations of decisions in the extraction process can produce models that accurately predict most of the known metabolic functionalities in the four cell lines. However, the tryptophan and phosphatidylinositol usage represent functions that were missed in most models for several reasons including the selection of a generic threshold for all reactions, incomplete or non-existent GPRs, imprecise quantification of exometabolomics, and the steady-state assumptions of the algorithms. Many of these concerns could be addressed in future algorithm development to allow MEMs to more comprehensively predict metabolic functionalities de novo for a cell line or tissue.

## DISCUSSION

Several methods have been developed to extract context-specific models from GEMs. Here we investigated the extraction procedure of cell line- or tissue-specific metabolic models. We compared and contrasted hundreds of models that were constructed using transcriptomics and exometabolomics data with several different combinations of algorithms (Table 1) and parameters (Figure 1A). Through this we showed that human cell-line-specific models more accurately predict the cell genotype-phenotype relationship than GEMs. We further quantified the influence of key decisions on model prediction accuracy and identified assumptions that limit the metabolic functionalities of a model. These analyses lead to important insights to consider when constructing context-specific models (Table 2). Thus, this study highlights (1) the importance of including diverse data types for model construction and validation, (2) the influence of select-

ing gene expression thresholds, and (3) the need for refinements to MEMs to construct more accurate context-specific models.

Our analysis showed that the decision of how to constrain the uptake and secretion fluxes in the model prior to model extraction has a lesser effect on the accuracy of gene-essentiality prediction than the other decisions. However, the use of proper constraints influences the capacity of the model to recover metabolic functionality when they were not defined a priori. Furthermore, uptake constraint selection significantly affected the ability to predict growth rates (see STAR Methods). Therefore, the development of more physiologically accurate models will be accelerated, when substrate consumption rates are determined and used. Beyond exometabolomics data, more diverse data are available to improve model content and validate model simulations. For example, the use of endometabolomic data (such as normally permitted by INIT) can be of great interest to capture key metabolite dynamics and allow their inclusion in extracted models. Doing so, the extraction process will gain in predictive power of some important metabolic features and help to drive discovery of metabolic functionalities of specific cell lines and tissues.

More so than constraint selection, the choice of the gene expression threshold at which a gene is considered “expressed” had the highest impact on model content (Figure 2C) and the ability to predict metabolic functionalities without predefining them (Figure 4C). However, the question remains on how to select the best threshold. A seemingly intuitive approach to avoid an arbitrary selection would be to select a threshold based on housekeeping genes, but some important housekeeping genes have low expression (Eisenberg and Levanon, 2013). Thus, it remains unclear how to use such genes to define a threshold (Figure S9). To address the challenge of identifying a reasonable threshold in our study, we compared model simulations with genome-wide loss-of-function screens. Our analysis suggests that stringent thresholds lead to more accurate gene-essentiality predictions. However, this improvement in accuracy comes at a cost, since smaller models with more stringent thresholds have fewer metabolic functions, if all relevant metabolic functions are not enforced a priori (Figure S10). Thus, if metabolic functions are known, more stringent thresholds should be considered. However, if the aim is to include previously unknown metabolic functions, lower thresholds could be considered, but external data should be used to evaluate the validity of predicted model functions (e.g., using knockout phenotypes, metabolomics, or fluxomics). Finally, we note that to ensure a consistent comparison of methods, we used a single threshold value. However, iMAT, for example, was originally designed to use two different

(C) The gene expression threshold contributes the most to the first PC for all cell lines with a lesser contribution of MEM choice. Meanwhile, the model constraint selection dominates the second PC. Error bars indicate SE across the four cell lines.

(D–F) Some metabolic functions failed to be added to most models, such as the synthesis of phosphatidylinositol and availability of tryptophan. (D) Phosphatidylinositol cannot be obtained from the model if the upstream reactions or metabolites are missing. A pie chart demonstrates the fraction of all 240 models that can synthesize phosphatidylinositol (purple, 39% of models) or cannot do so (blue, 61%). Models fail to predict the phosphatidylinositol functionality if the CDIPT<sub>r</sub> reaction (synthesizes the metabolite) is absent (green, 19%) or when the required upstream substrates for CDIPT<sub>r</sub> are missing, such as CDP diacylglycerol and/or inositol (gray). (E) Even when these reactions or metabolites are missing, phosphatidylinositol is often found in the model in a metabolic cycle since individual enzymes in the cycle are expressed. However, with no input into the cycle, phosphatidylinositol cannot leave the cycle at steady state and contribute to the metabolic function. (F) Tryptophan is unavailable in most models since (1) the algorithms often remove reactions without known genes (e.g., TRPt, EX\_trp-L (e), etc.), (2) the GPR of a key reaction was incomplete (TRPO2), and (3) too many reactions in the pathways using the metabolite have low expression. See Table S2 for metabolite and reaction abbreviations.

**Table 2. Considerations for the Construction of Context-Specific Models**

Model Attribute	Decision Most Strongly Affecting Attribute (% Variation Explained)	Concerns	Perspectives
Model content (size, completeness)	Threshold (65%, PC1)	<ul style="list-style-type: none"> <li>● Less stringent thresholds typically lead to decreased power to predict essential versus non-essential genes.</li> <li>● Uniform thresholds do not capture the continuous nature of enzyme abundance.</li> <li>● Model content can be limited by missing GPRs.</li> </ul>	<ul style="list-style-type: none"> <li>● More reliable models can be obtained by identifying a threshold that maximizes the consistency of model predictions with validation data (e.g., gene essentiality, fluxes, etc.).</li> <li>● Gene- or reaction-specific thresholds could be defined with the use of gene-specific properties (e.g., enzyme kinetics, expression across many conditions, expression of neighboring genes in the same pathways).</li> <li>● Known metabolic functionalities can be imposed to force the inclusion of pathways with incomplete GPRs or enzymes with low expression.</li> </ul>
Metabolic functionality	Threshold (51%, PC1)	<ul style="list-style-type: none"> <li>● Stringent thresholds will lead to the elimination of functionalities unless they are pre-specified.</li> <li>● Algorithms can eliminate highly expressed reactions if neighboring genes have low expression.</li> <li>● Inadequate constraints can lead to an inability to predict and recapitulate metabolic functions.</li> <li>● Some MEMs inherently lead to smaller models with fewer functionalities.</li> </ul>	<ul style="list-style-type: none"> <li>● Additional data should be used to define as many functions <i>a priori</i> (e.g., genetic screens, exometabolomics, cell composition analysis, endometabolomics data, etc.).</li> <li>● If metabolic functions are unknown, low thresholds can be allowed, but metabolic functions must be verified using different data types (e.g., fluxomics, metabolomics, gene knock down/knock out).</li> <li>● Well-defined metabolite uptake and secretion rates can be imposed to avoid metabolic function elimination.</li> </ul>
Gene essentiality	MEM (40%)	<ul style="list-style-type: none"> <li>● Some essential metabolic functions are needed at low amounts and so enzymes show low expression. Thus, MEM reaction removal criteria may cause false-positive essential genes.</li> <li>● To meet an essential function, many MEMs randomly remove reactions when multiple pathways with a low expression reaction exist, thus leading to other reactions becoming essential.</li> <li>● Most model-predicted essential genes are binary growth/no-growth calls and miss more subtle changes in growth rate.</li> </ul>	<ul style="list-style-type: none"> <li>● Defining a core set of reactions that are known to be active, plus metabolic functions that must be tested, ensures that essential processes are covered by the model and improve essentiality calls.</li> <li>● Development of methods that use gene-specific thresholds or enzyme kinetics may identify actual pathways that should be removed, thereby ensuring that essential genes remain in the model.</li> </ul>

thresholds to differentiate high, medium, and low expression. Thus, more advanced users can use the workflow we presented here to test the impact of these additional parameters.

While we show that threshold selection can be optimized with the use of additional data, the wide range of expression levels of housekeeping genes suggests future algorithms need to look beyond the use of a global expression threshold to define tissue-specific genes. A global threshold ignores the diverse ranges of activity for different enzymes, stemming from their different catalytic efficiencies and differences in required expression levels. We anticipate that more accurate models of tissue-

specific metabolism will be obtained with novel approaches that use gene-specific expression thresholds, information on enzyme kinetic parameters, and/or information on the required magnitude of fluxes for biological functions. Recent studies are starting to approach this goal by including more gene-specific constraints (Yizhak et al., 2014; Robaina Estévez and Nikoloski, 2015), although much work remains in this space.

We demonstrated here that the context-specific models can accurately predict gene-essentiality, as has been successfully done in *E. coli* (Edwards and Palsson, 2000), yeast (Heavner et al., 2013), and other microbes. Interestingly, the choice of a

MEM itself has the greatest impact on the accuracy of the gene-essentiality predictions. Thus, great care must be taken when selecting which algorithm to use. Careful thought must be taken to consider the assumptions and requirements of an algorithm. For gene-essentiality and functionality predictions, we found that starting with a set of core reactions and known functionalities considerably improves model accuracy. We also observed that some models are not able to capture all metabolic functions (e.g., tryptophan and phosphatidylinositol usage) due to limitations of current algorithms used for extraction (e.g., requirements to remove pathways if neighboring reactions have unknown or inaccurate GPRs). However, it is expected that improvements to algorithmic assumptions will lead to better predictions, such as metabolic anti-cancer targets or the unique and previously unreported metabolic functions of individual tissues or cell lines.

Finally, all of these efforts require improved characterization of metabolism. Gaps in our knowledge of human metabolism must be filled through integrated computational and experimental efforts (Rolfsson et al., 2011). This will include genetic screens, such as genome-wide CRISPR-Cas9 screens, algorithms that enable rapid discovery of gap filling strategies, and biochemical characterization of enzymes. Finally, there is a need for the detailed definition of the metabolic functions of tissues and individual cell types. When a cell is known to have certain functionalities, it helps to enforce their inclusion during model extraction (such as done in INIT [Agren et al., 2014] and mCADRE). Together, these efforts will improve tissue-specific metabolic modeling.

## Conclusion

Context-specific models depend substantially on key decisions on methodology and data processing, and these decisions significantly influence their size, functionality, and accuracy. While there is no strong evidence that one MEM universally gives the most physiologically accurate models, each method has different underlying assumptions that affect the resulting model. Therefore, selection of the MEM and the associated parameters should be done while considering the goals of the study and the available data. This comparative analysis of extraction methods and relevant parameters highlights that the use of omic data can aid in the construction of tissue-specific models. These models can improve the predictive capacity of genotype-phenotype relationships (evaluated through known metabolic functions and gene essentiality in the context of this study). However, care must be taken to build the most accurate models. Furthermore, advances in algorithmic development, inclusion of additional data, and refinement of the human genome-scale metabolic network reconstruction will be needed to further improve the accuracy of such models. Such efforts will continue to increase in value for systems biology analyses and biomedical applications.

## STAR★METHODS

Detailed methods are provided in the online version of this paper and include the following:

- KEY RESOURCES TABLE
- CONTACT FOR REAGENT AND RESOURCE SHARING

## ● METHOD DETAILS

- Implementation of the MEMs
- Curation of the Exometabolomic Data
- Determination of the Biomass Reaction
- Constraining the Input Models
- RNA-Seq Data Processing
- Processing of the Knockout Screen Data
- Predictions of Gene-Essentiality
- Calculating the Functionality Score
- Extraction of Cell Line-specific Models Using the MEMs
- Results from Recon1 Are Generalizable to Other Human Reconstructions
- MILP-Based MEMs Have Multiple Solutions Performing Equivalently
- Minor Changes to the Biomass Composition Does Not Significantly Influence Gene Essentiality Results
- Extracted Models Do Not Inherently Predict Growth Rates

## ● QUANTIFICATION AND STATISTICAL ANALYSIS

- Principal Component Analysis

## ● DATA AND SOFTWARE AVAILABILITY

## SUPPLEMENTAL INFORMATION

Supplemental Information includes 12 figures, 7 tables, and 1 data file and can be found with this article online at <http://dx.doi.org/10.1016/j.cels.2017.01.010>.

## AUTHOR CONTRIBUTIONS

S.O., A.R., and N.E.L. designed the study, conducted the analyses, and wrote the paper. S.L. and B.K. analyzed data. D.C.Z. analyzed metabolomics data and developed the biomass function. All authors have read and approved the work.

## ACKNOWLEDGMENTS

This work was supported by generous funding from the Novo Nordisk Foundation provided to the Center for Biosustainability at the Technical University of Denmark (grant no. NNF16CC0021858), and from NIGMS (grant no. R35 GM119850). We also thank the W.M. Keck Foundation for generous funding that enabled this work.

Received: June 12, 2016

Revised: November 26, 2016

Accepted: January 12, 2017

Published: February 15, 2017

## REFERENCES

- Agren, R., Bordel, S., Mardinoglu, A., Pornputtapong, N., Nookaew, I., and Nielsen, J. (2012). Reconstruction of genome-scale active metabolic networks for 69 human cell types and 16 cancer types using INIT. *PLoS Comput. Biol.* 8, e1002518.
- Agren, R., Liu, L., Shoaie, S., Vongsangnak, W., Nookaew, I., and Nielsen, J. (2013). The RAVEN toolbox and its use for generating a genome-scale metabolic model for *Penicillium chrysogenum*. *PLoS Comput. Biol.* 9, e1002980.
- Agren, R., Mardinoglu, A., Asplund, A., Kampf, C., Uhlen, M., and Nielsen, J. (2014). Identification of anticancer drugs for hepatocellular carcinoma through personalized genome-scale metabolic modeling. *Mol. Syst. Biol.* 10, 1–13.
- Altamirano, C., Illanes, A., Casablancas, A., Gámez, X., Cairó, J.J., and Gòdia, C. (2001). Analysis of CHO cells metabolic redistribution in a glutamate-based defined medium in continuous culture. *Biotechnol. Prog.* 17, 1032–1041.

- Becker, S.A., and Palsson, B.O. (2008). Context-specific metabolic networks are consistent with experiments. *PLoS Comput. Biol.* *4*, e1000082.
- Bolger, A.M., Lohse, M., and Usadel, B. (2014). Trimmomatic: a flexible trimmer for Illumina sequence data. *Bioinformatics* *30*, 2114–2120.
- Bonarius, H.P., Hatzimanikatis, V., Meesters, K.P., de Gooijer, C.D., Schmid, G., and Tramper, J. (1996). Metabolic flux analysis of hybridoma cells in different culture media using mass balances. *Biotechnol. Bioeng.* *50*, 299–318.
- Bordbar, A., Monk, J.M., King, Z.A., and Palsson, B.O. (2014). Constraint-based models predict metabolic and associated cellular functions. *Nat. Rev. Genet.* *15*, 107–120.
- Bürkstümmer, T., Banning, C., Hainzl, P., Schobesberger, R., Kerzendorfer, C., Pauler, F.M., Chen, D., Them, N., Schischlik, F., Rebsamen, M., et al. (2013). A reversible gene trap collection empowers haploid genetics in human cells. *Nat. Methods* *10*, 965–971.
- Covert, M.W., Knight, E.M., Reed, J.L., Herrgard, M.J., and Palsson, B.O. (2004). Integrating high-throughput and computational data elucidates bacterial networks. *Nature* *429*, 92–96.
- De Menezes, Y., De Faria, F.P., and Sesso, A. (1996). In human hepatocellular carcinoma cells the total membrane surface area of each major organelle is a particular allometric function of the cytoplasmic volume. A morphometric study. *J. Submicrosc. Cytol. Pathol.* *28*, 573–582.
- Di Ruscio, A., Ebralidze, A.K., Benoukraf, T., Amabile, G., Goff, L.A., Terragni, J., Figueroa, M.E., De Figueiredo Pontes, L.L., Alberich-Jorda, M., Zhang, P., et al. (2013). DNMT1-interacting RNAs block gene-specific DNA methylation. *Nature* *503*, 371–376.
- Dobin, A., Davis, C.A., Schlesinger, F., Drenkow, J., Zaleski, C., Jha, S., Batut, P., Chaisson, M., and Gingeras, T.R. (2013). STAR: ultrafast universal RNA-seq aligner. *Bioinformatics* *29*, 15–21.
- Dolfi, S.C., Chan, L.L.-Y., Qiu, J., Tedeschi, P.M., Bertino, J.R., Hirshfield, K.M., Oltvai, Z.N., and Vazquez, A. (2013). The metabolic demands of cancer cells are coupled to their size and protein synthesis rates. *Cancer Metab.* *1*, 20.
- Duarte, N.C., Becker, S.A., Jamshidi, N., Thiele, I., Mo, M.L., Vo, T.D., Srivas, R., and Palsson, B.O. (2007). Global reconstruction of the human metabolic network based on genomic and bibliomic data. *Proc. Natl. Acad. Sci. USA* *104*, 1777–1782.
- Edwards, J.S., and Palsson, B.O. (2000). The *Escherichia coli* MG1655 in silico metabolic genotype: its definition, characteristics, and capabilities. *Proc. Natl. Acad. Sci. USA* *97*, 5528–5533.
- Eisenberg, E., and Levanon, E.Y. (2013). Human housekeeping genes, revisited. *Trends Genet.* *29*, 569–574.
- Feijó Delgado, F., Cermak, N., Hecht, V.C., Son, S., Li, Y., Knudsen, S.M., Olcum, S., Higgins, J.M., Chen, J., Grover, W.H., and Manalis, S.R. (2013). Intracellular water exchange for measuring the dry mass, water mass and changes in chemical composition of living cells. *PLoS One* *8*, e67590.
- Folger, O., Jerby, L., Frezza, C., Gottlieb, E., Ruppin, E., and Shlomi, T. (2011). Predicting selective drug targets in cancer through metabolic networks. *Mol. Syst. Biol.* *7*, 501.
- Frezza, C., Zheng, L., Folger, O., Rajagopalan, K.N., MacKenzie, E.D., Jerby, L., Micaroni, M., Chaneton, B., Adam, J., Hedley, A., et al. (2011). Haem oxygenase is synthetically lethal with the tumour suppressor fumarate hydratase. *Nature* *477*, 225–228.
- Frixione, E., and Porter, R.M. (1986). Volume and surface changes of smooth endoplasmic reticulum in crayfish retinula cells upon light- and dark-adaptation. *J. Comp. Physiol. A* *159*, 667–674.
- Gatto, F., Miess, H., Schulze, A., and Nielsen, J. (2015). Flux balance analysis predicts essential genes in clear cell renal cell carcinoma metabolism. *Sci. Rep.* *5*, 10738.
- Gout, P.W., Kang, Y.J., Buckley, D.J., Bruchovsky, N., and Buckley, A.R. (1997). Increased cystine uptake capability associated with malignant progression of Nb2 lymphoma cells. *Leukemia* *11*, 1329–1337.
- Heavner, B.D., Smallbone, K., Price, N.D., and Walker, L.P. (2013). Version 6 of the consensus yeast metabolic network refines biochemical coverage and improves model performance. *Database (Oxford)* *2013*, 1–5.
- Ho Sui, S.J., Lo, R., Fernandes, A.R., Caulfield, M.D.G., Lerman, J.A., Xie, L., Bourne, P.E., Baillie, D.L., and Brinkman, F.S.L. (2012). Raloxifene attenuates *Pseudomonas aeruginosa* pyocyanin production and virulence. *Int. J. Antimicrob. Agents* *40*, 246–251.
- Hyduke, D.R., Lewis, N.E., and Palsson, B.O. (2013). Analysis of omics data with genome-scale models of metabolism. *Mol. Biosyst.* *9*, 167–174.
- Jain, M., Nilsson, R., Sharma, S., Madhusudhan, N., Kitami, T., Souza, A.L., Kafri, R., Kirschner, M.W., Clish, C.B., and Mootha, V.K. (2012). Metabolite profiling identifies a key role for glycine in rapid cancer cell proliferation. *Science* *336*, 1040–1044.
- Jerby, L., Shlomi, T., and Ruppin, E. (2010). Computational reconstruction of tissue-specific metabolic models: application to human liver metabolism. *Mol. Syst. Biol.* *6*, 401.
- Kilburn, D.G., Lilly, M.D., and Webb, F.C. (1969). The energetics of mammalian cell growth. *J. Cell Sci.* *4*, 645–654.
- Kim, H.U., Kim, S.Y., Jeong, H., Kim, T.Y., Kim, J.J., Choy, H.E., Yi, K.Y., Rhee, J.H., and Lee, S.Y. (2014). Integrative genome-scale metabolic analysis of *Vibrio vulnificus* for drug targeting and discovery. *Mol. Syst. Biol.* *7*, 460.
- King, Z.A., Lu, J., Dräger, A., Miller, P., Federowicz, S., Lerman, J.A., Ebrahim, A., Palsson, B.O., and Lewis, N.E. (2016). BiGG Models: a platform for integrating, standardizing and sharing genome-scale models. *Nucleic Acids Res.* *44*, D515–D522.
- Kit, S., Fiscus, J., Graham, O.L., and Gross, A.L. (1959). Metabolism and enzyme content of diploid and tetraploid lymphomas and carcinomas. *Cancer Res.* *19*, 201–206.
- Lewis, N.E., and Abdel-Haleem, A.M. (2013). The evolution of genome-scale models of cancer metabolism. *Front. Physiol.* *4*, 237.
- Lewis, N.E., Schramm, G., Bordbar, A., Schellenberger, J., Andersen, M.P., Cheng, J.K., Patel, N., Yee, A., Lewis, R.A., Eils, R., et al. (2010). Large-scale in silico modeling of metabolic interactions between cell types in the human brain. *Nat. Biotechnol.* *28*, 1279–1285.
- Lewis, N.E., Nagarajan, H., and Palsson, B.O. (2012). Constraining the metabolic genotype-phenotype relationship using a phylogeny of in silico methods. *Nat. Rev. Microbiol.* *10*, 291–305.
- Mahadevan, R., and Schilling, C.H. (2003). The effects of alternate optimal solutions in constraint-based genome-scale metabolic models. *Metab. Eng.* *5*, 264–276.
- Mardinoglu, A., Agren, R., Kampf, C., Asplund, A., Uhlen, M., and Nielsen, J. (2014). Genome-scale metabolic modelling of hepatocytes reveals serine deficiency in patients with non-alcoholic fatty liver disease. *Nat. Commun.* *5*, 3083.
- Mudunuri, U., Che, A., Yi, M., and Stephens, R.M. (2009). bioDBnet: the biological database network. *Bioinformatics* *25*, 555–556.
- Noor, E., Lewis, N.E., and Milo, R. (2012). A proof for loop-law constraints in stoichiometric metabolic networks. *BMC Syst. Biol.* *6*, 140.
- Pacheco, M.P., Pfau, T., and Sauter, T. (2015). Benchmarking procedures for high-throughput context specific reconstruction algorithm. *Front. Physiol.* *6*, 410.
- Pawlikowski, J.S., McBryan, T., van Tuyn, J., Drotar, M.E., Hewitt, R.N., Maier, A.B., King, A., Blyth, K., Wu, H., and Adams, P.D. (2013). Wnt signaling potentiates neovogenesis. *Proc. Natl. Acad. Sci. USA* *110*, 16009–16014.
- Prendergast, G.C. (2011). Cancer: why tumours eat tryptophan. *Nature* *478*, 192–194.
- Quek, L.-E., Dietmar, S., Hanscho, M., Martínez, V.S., Borth, N., and Nielsen, L.K. (2014). Reducing Recon 2 for steady-state flux analysis of HEK cell culture. *J. Biotechnol.* *184*, 172–178.
- Robaina Estévez, S., and Nikoloski, Z. (2014). Generalized framework for context-specific metabolic model extraction methods. *Front. Plant Sci.* *5*, 1–11.
- Robaina Estévez, S., and Nikoloski, Z. (2015). Context-specific metabolic model extraction based on regularized least squares optimization. *PLoS One* *10*, e0131875.

- Rolfsson, O., Palsson, B.Ø., and Thiele, I. (2011). The human metabolic reconstruction Recon 1 directs hypotheses of novel human metabolic functions. *BMC Syst. Biol.* 5, 155.
- Roschke, A.V., Tonon, G., Gehlhaus, K.S., McTyre, N., Bussey, K.J., Lababidi, S., Scudiero, D.A., Weinstein, J.N., and Kirsch, I.R. (2003). Karyotypic complexity of the NCI-60 drug-screening panel. *Cancer Res.* 63, 8634–8647.
- Schellenberger, J., Que, R., Fleming, R.M.T., Thiele, I., Orth, J.D., Feist, A.M., Zielinski, D.C., Bordbar, A., Lewis, N.E., Rahmanian, S., et al. (2011). Quantitative prediction of cellular metabolism with constraint-based models: the COBRA Toolbox v2.0. *Nat. Protoc.* 6, 1290–1307.
- Shalem, O., Sanjana, N.E., Hartenian, E., Shi, X., Scott, D.A., Mikkelsen, T.S., Heckl, D., Ebert, B.L., Root, D.E., Doench, J.G., and Zhang, F. (2014). Genome-scale CRISPR-Cas9 knockout screening in human cells. *Science* 343, 84–87.
- Sheikh, K., Förster, J., and Nielsen, L.K. (2005). Modeling hybridoma cell metabolism using a generic genome-scale metabolic model of *Mus musculus*. *Biotechnol. Prog.* 21, 112–121.
- Shen, Y., Liu, J., Estiu, G., Isin, B., Ahn, Y.-Y., Lee, D.-S., Barabási, A.-L., Kapatral, V., Wiest, O., and Oltvai, Z.N. (2010). Blueprint for antimicrobial hit discovery targeting metabolic networks. *Proc. Natl. Acad. Sci. USA* 107, 1082–1087.
- Shlomi, T., Cabili, M.N., Herrgård, M.J., Palsson, B.Ø., and Ruppin, E. (2008). Network-based prediction of human tissue-specific metabolism. *Nat. Biotechnol.* 26, 1003–1010.
- Swainston, N., Smallbone, K., Hefzi, H., Dobson, P.D., Brewer, J., Hanscho, M., Zielinski, D.C., Ang, K.S., Gardiner, N.J., Gutierrez, J.M., et al. (2016). Recon 2.2: from reconstruction to model of human metabolism. *Metabolomics* 12, 109.
- Thiele, I., Swainston, N., Fleming, R.M.T., Hoppe, A., Sahoo, S., Aurich, M.K., Haraldsdottir, H., Mo, M.L., Rolfsson, O., Stobbe, M.D., et al. (2013). A community-driven global reconstruction of human metabolism. *Nat. Biotechnol.* 31, 419–425.
- Trapnell, C., Williams, B.A., Pertea, G., Mortazavi, A., Kwan, G., van Baren, M.J., Salzberg, S.L., Wold, B.J., and Pachter, L. (2011). Transcript assembly and abundance estimation from RNA-seq reveals thousands of new transcripts and switching among isoforms. *Nat. Biotechnol.* 28, 511–515.
- Uhlen, M., Fagerberg, L., Hallstrom, B.M., Lindskog, C., Oksvold, P., Mardinoglu, A., Sivertsson, A., Kampf, C., Sjostedt, E., Asplund, A., et al. (2015). Tissue-based map of the human proteome. *Science* 347, 1260419.
- Vivanco, I., and Sawyers, C.L. (2002). The phosphatidylinositol 3-Kinase AKT pathway in human cancer. *Nat. Rev. Cancer* 2, 489–501.
- Vlassis, N., Pacheco, M.P., and Sauter, T. (2014). Fast reconstruction of compact context-specific metabolic network models. *PLoS Comput. Biol.* 10, e1003424.
- Wang, Y., Eddy, J.A., and Price, N.D. (2012). Reconstruction of genome-scale metabolic models for 126 human tissues using mCADRE. *BMC Syst. Biol.* 6, 153.
- Wang, T., Wei, J.J., Sabatini, D.M., and Lander, E.S. (2014). Genetic screens in human cells using the CRISPR-Cas9 system. *Science* 343, 80–84.
- Wang, T., Birsoy, K., Hughes, N.W., Krupczak, K.M., Post, Y., Wei, J.J., Lander, E.S., and Sabatini, D.M. (2015). Identification and characterization of essential genes in the human genome. *Science* 350, 1096–1101.
- Yang, H., Krumholz, E.W., Brutinel, E.D., Palani, N.P., Sadowsky, M.J., Odlyzko, A.M., Gralnick, J.A., and Libourel, I.G.L. (2014). Genome-scale metabolic network validation of *Shewanella oneidensis* using transposon insertion frequency analysis. *PLoS Comput. Biol.* 10, e1003848.
- Yizhak, K., Gaude, E., Le Dévédéc, S., Waldman, Y.Y., Stein, G.Y., van de Walter, B., Frezza, C., and Ruppin, E. (2014). Phenotype-based cell-specific metabolic modeling reveals metabolic liabilities of cancer. *Elife* 3, e03641.
- Yizhak, K., Chaneton, B., Gottlieb, E., and Ruppin, E. (2015). Modeling cancer metabolism on a genome scale. *Mol. Syst. Biol.* 11, 817.
- Yuan, H., Cheung, C.Y.M., Hilbers, P.A.J., and van Riel, N.A.W. (2016). Flux balance analysis of plant metabolism: the effect of biomass composition and model structure on model predictions. *Front. Plant Sci.* 7, 537.
- Zhang, J., Lieu, Y.K., Ali, A.M., Penson, A., Reggio, K.S., Rabadan, R., Raza, A., Mukherjee, S., and Manley, J.L. (2015). Disease-associated mutation in SRSF2 misregulates splicing by altering RNA-binding affinities. *Proc. Natl. Acad. Sci. USA* 112, E4726–E4734.
- Zur, H., Ruppin, E., and Shlomi, T. (2010). iMAT: an integrative metabolic analysis tool. *Bioinformatics* 26, 3140–3142.

## STAR★METHODS

### KEY RESOURCES TABLE

Reagent or Resource	Source	Identifier
<b>Deposited Data</b>		
mRNA-sequencing datasets for KBM7	<a href="#">Bürckstümmer et al., 2013</a>	GEO: GSE48848
mRNA-sequencing datasets for HL60	<a href="#">Di Ruscio et al., 2013</a>	GEO: GSE41279
mRNA-sequencing datasets for A375	<a href="#">Pawlikowski et al., 2013</a>	GEO: GSE46818
mRNA-sequencing datasets for K562	<a href="#">Zhang et al., 2015</a>	GEO: GSE71299
Exometabolomics data for NCI-60	<a href="#">Jain et al., 2012</a>	PMID: 22628656
Genome-scale CRISPR-Cas9 knockout screens	<a href="#">Shalem et al., 2014</a> ; <a href="#">Wang et al., 2014, 2015</a>	PMID: 24336571 PMID: 26472758 PMID: 24336569
<b>Software and Algorithms</b>		
Trimmomatic	<a href="#">Bolger et al., 2014</a>	<a href="http://www.usadellab.org">www.usadellab.org</a>
STAR	<a href="#">Dobin et al., 2013</a>	<a href="http://code.google.com/archive/p/rna-star">code.google.com/archive/p/rna-star</a>
Cufflinks	<a href="#">Trapnell et al., 2011</a>	<a href="http://cufflinks.cbc.umd.edu">cufflinks.cbc.umd.edu</a>
bioDBnet 2.0	<a href="#">Mudunuri et al., 2009</a>	<a href="http://biodbnet-abcc.ncifcrf.gov">biodbnet-abcc.ncifcrf.gov</a>
fastCC	<a href="#">Vlassis et al., 2014</a>	PMID: 24453953
COBRA Toolbox 2.0	<a href="#">Schellenberger et al., 2011</a>	PMID: 21886097
<b>Other</b>		
Recon1 model	<a href="#">Duarte et al., 2007</a>	<a href="http://bigg.ucsd.edu">bigg.ucsd.edu</a>
Recon 2.2 model	<a href="#">Swainston et al., 2016</a>	PMID: 27358602
BiGG Database	<a href="#">King et al., 2016</a>	<a href="http://bigg.ucsd.edu">bigg.ucsd.edu</a>

### CONTACT FOR REAGENT AND RESOURCE SHARING

Further information and requests for reagents may be directed to, and will be fulfilled by the corresponding author, Dr. N.E. Lewis ([nlewisres@ucsd.edu](mailto:nlewisres@ucsd.edu)).

### METHOD DETAILS

#### Implementation of the MEMs

##### **FASTCORE**

The implementation of FASTCORE ([Vlassis et al., 2014](#)) is freely available at [http://bio.uni.lu/systems\\_biology/software/](http://bio.uni.lu/systems_biology/software/). The only alterations made for this study were the use of Gurobi instead of CPLEX as a solver and the change of an internal scaling constant to  $1 \times 10^3$ , when it was originally  $1 \times 10^5$ . This was necessary to allow the algorithm to adequately determine whether a reaction was active when small-valued constraints are present. The gene expression thresholds were used to determine the core reactions set. Reactions without expression data were never considered core reactions. The biomass reaction and ATP demand reaction were always added to the set of core reactions except when models were extracted for evaluation of the metabolic functionalities.

##### **GIMME**

The implementation of GIMME is a slightly modified version of the implementation from the COBRA toolbox. In this study, the gene expression data were not discretized but the expression levels were used directly as weights in the objective function, as done in the original publication of GIMME ([Becker and Palsson, 2008](#)). The gene expression threshold was subtracted from the expression for the reactions, thus determining whether it would be assigned a positive or negative weight in the objective. Reactions without expression data were given a weight of zero. The minimal fraction of the biomass objective value was set to 90%.

##### **iMAT**

In the original version of iMAT ([Shlomi et al., 2008](#)), three sets of reactions were defined (“high expression”, “low expression” and “moderately expressed/no data”). To maintain consistency and simplify comparison with the other extraction methods, we merged low and high expressed sets into a single group. All reactions without expression data were put in the “moderately expressed/no data” reaction set. The biomass reaction and ATP demand reaction were always added to the “high expression” reaction set, except when models were extracted for evaluation of the metabolic functionalities. When the unconstrained or semi-constrained model was

used as input, the flux activation threshold ( $\epsilon$ ) was set to 1, which was also done in the original publication. When the constrained model was used as input, a flux activation threshold of  $1 \times 10^{-6}$  was used. This value was chosen because it is smaller than the smallest exchange reaction constraint but still larger than the threshold of  $1 \times 10^{-8}$ , used to define consistent reactions. A maximum solve time of one hour was used for the MILP for the unconstrained and semi-constrained input models. This was increased to two hours for the constrained input model. After this time the solution was always near-optimal (<10% variation around the best known objective value). Equivalent optimal models could be acquired, but when different models from the same parameter set were analyzed, they provide qualitatively similar results (Figures S3 and S4).

### INIT

An implementation of INIT is provided in the RAVEN toolbox (Agren et al., 2013). However, this implementation is meant to work with models that are structured in a slightly different manner than the COBRA models. Moreover, the accumulation of metabolites as used in the original version of INIT (Agren et al., 2012) was not used here because we did not have endometabolomics data for the cell lines. Thus, after the simplification, each reaction was given a (non-zero) weight according to Equation 1. Reactions with positive weights were put in the “high expression” set and reactions with negative weights were put in the “low expression” set. Reactions with missing expression data were given a weight of -2. The biomass reaction and ATP demand reaction were assigned a weight equal to the maximum across all reactions, except when models were extracted for evaluation of the metabolic functionalities (see Methods). These methods of weighting are similar to those used in the original publication of INIT. The objective of the resulting MILP was a maximization of the sum of weights. Specifically, the weight of a high-expression-reaction was added when it was active and the absolute value of the weight of a low-expression-reaction was added when it was inactive. The flux activation thresholds were the same as used for iMAT. A maximum solve time of one hour was used for the MILP for the unconstrained and semi-constrained input models. This was increased to two hours for the constrained input model. After this time the solution was always near-optimal (<10% variation around the best known objective value).

$$weight = 5 \cdot \log\left(\frac{Expression\ level}{Threshold}\right) \quad (\text{Equation 1})$$

Assignment of weights for INIT. As logarithms for very small expression levels can approach  $-\infty$ , a minimum weight equal to the negative of the maximum weight across the reactions was used.

### MBA

Implementation of MBA followed the pseudo-code in the publication (Jerby et al., 2010). The gene expression threshold was used to determine the high-confidence reaction set. The medium confidence reactions set was always left empty such that only one expression threshold was used to maintain consistency with other methods. The biomass reaction and ATP demand reaction were always added to the high-confidence reactions set, except when models were extracted for evaluation of the metabolic functionalities. Since MBA prunes reactions in a random order, output models may differ even when the input was identical. Thus, while multiple models were built, the analyses in the paper used only 1 randomly chosen one for each set of parameters, unless specified otherwise. However, results were qualitatively similar for different models constructed with the same parameter set (Figures S3 and S4).

### mCADRE

The implementation of mCADRE is freely available at <https://github.com/jaedydy/mcadre>. Originally, mCADRE used microarray data as input to determine which reactions should be in the core. Here, we used RNA-Seq. The gene expression threshold of the RNA-Seq data was used to determine the set of core reactions. The biomass reaction and ATP demand reaction was always added to the set of core reactions, except when models were extracted for evaluation of the metabolic functionalities (see Methods). Reactions with zero expression were given a negative expression value and reactions with no GPRs or no measured expression data will be given an expression of zero. Then, all reactions that were not in the core were ordered with respect to their expression, their connectivity score, and their confidence score, respectively. The ratio of inactivated core reactions to inactivated non-core reactions was set to 1/3, as done in the original publication (Wang et al., 2012). The metabolic function and salvage pathway checks that were standard in mCADRE were also used.

### Curation of the Exometabolomic Data

Published metabolite uptake and release (exometabolomic) data on the NCI-60 lines (Jain et al., 2012) was re-processed in a semi-automated process. The original dataset was processed by correcting for drift in the peak area standardization across runs. This was done by a linear L1 regression of blank media standards. However, upon detailed inspection of the drift for different metabolites, it was apparent that the drift was highly non-linear for some metabolites. The effect of applying a linear approximation in these non-linear cases was that metabolite uptakes were significantly misrepresented, and in some cases, metabolites were actually not exchanged substantially at all, once a non-linear drift correction was applied. We manually created non-linear approximations of drift for each metabolite in Mathematica based on the media standards for each metabolite. We applied these non-linear corrections to the raw data to recalculate the metabolite uptake and release profiles.

The metabolites from the exometabolomics data used in this study were previously measured in the media using LC-MS/MS. The absolute concentrations were determined using standards for each metabolite. Metabolites were identified based on having the same m/z values and LC retention times as standards, as described previously (Jain et al., 2012).

### Determination of the Biomass Reaction

Cell biomass is composed of protein, lipids, DNA, RNA and small molecules, in weight fractions determined by cell composition studies (Table S1). The average amino acid composition of protein was taken from literature (Altamirano et al., 2001; Bonarius et al., 1996; Sheikh et al., 2005). Approximate DNA deoxyribonucleotide composition was set based on genomic base frequency, taking into account the karyotype of the NCI-60 lines (Roschke et al., 2003). RNA ribonucleotide composition was determined based on measured mass fractions (Altamirano et al., 2001; Bonarius et al., 1996; Sheikh et al., 2005). Lipid composition was set based on measured lipid composition for high concentration lipids. Small molecule weight fractions were determined for several high concentration non-essential metabolites using literature concentrations and a typical cell dry weight of 0.2 ng/cell and cell volume of 2 pL/cell when unit conversions were necessary.

We chose to set the macromolecule weight fractions to be constant between cell lines. Previous studies show minimal variance between macromolecule weight fractions for particular types of cells, such as hybridoma cells and Chinese hamster ovary cells (Altamirano et al., 2001; Bonarius et al., 1996; Sheikh et al., 2005). Other cell types, such as liver cells, may have significantly different macromolecule weight fractions, but cell lines derived from such tissues are not present in the NCI-60 panel. Also, although cell composition has also been reported to change across growth conditions (Feijó Delgado et al., 2013), the NCI-60 panel was subject to uniform growth conditions in the studies generating the data used in this study. Furthermore, there is the question of whether cell composition changes with cell size. One study showed that doubling of cell size resulted in approximate doubling of respiration, suggesting the protein content scales proportionally to size (Kit et al., 1959). Also, as volume changes, the cell surface area (SA) to volume (V) ratio changes, and thus it is possible that the lipid weight fraction of the cell changes as well. However, compartment size has been shown to be approximately linearly correlated with total volume (De Menezes et al., 1996), and ER membrane alone is reported to be over 10 times the fraction of the total membrane as the cytoplasmic membrane (Frixione and Porter, 1986), suggesting SAVV differences mean little in terms of lipid requirements. Thus, we assumed that the macromolecule composition was invariant across cell lines, although cell sizes differ. Protein content and cell volume data for the NCI-60 was recently published (Dolfi et al., 2013). However, these data were insufficient to set cell-specific biomass macromolecule weight fractions, since the cell dry weight was not measured.

To determine the cell-specific dry weights, we integrated cell volume data with the uptake rates as follows. First, the amount of biomass sustainable by each cell was determined by maximizing the growth for each cell line using FBA, while constrained by measured metabolite uptake rates in units of “per cell”. Then, this sustainable biomass was corrected using measured protein content data as follows. If the sustainable protein, taking protein as 0.70 of total cell dry mass, is less than the measured protein, a value of 95% of the sustainable protein measurement was used as the estimate of cellular protein. This was done because the measured protein could not be sustained by the measured uptake rates, which we assumed was due to error in the measured protein. Measured protein was assumed to be the greater source of error because the measured uptake rates are highly correlated and there was no general bias of sustainable protein being greater or less than measured protein. Furthermore, the measured protein showed a relatively low agreement with cell volumes (Pearson  $R^2 = 0.23$ ) and we observed certain spurious data points causing concern. For example, the SR line was reported to have a protein content of 0.021 ng/cell, which, given the reported cell volume and average protein density, would result in a dry weight fraction of protein of approximately 0.08, which is substantially lower than measured values around 0.7. Volume measurements were based in microscopy, and thus were seen as less error prone than protein content measurements which require cell count estimation, which can be a significant source of error. When sustainable protein was greater than measured protein, the measured value was used to correct the sustainable protein, using the formula:  $m_{\text{estimate}} = m_{\text{measured}} + 0.25 \cdot (m_{\text{sustainable}} - m_{\text{measured}})$ . This formula was chosen based on resulting agreement with cell volume data. The correlation of estimated protein content with cell volume (Pearson  $R^2 = 0.60$ ) was higher than either measured protein (Pearson  $R^2 = 0.23$ ) or sustainable protein (Pearson  $R^2 = 0.52$ ).

### Constraining the Input Models

Recon1 (Duarte et al., 2007) was downloaded from the BiGG Database (King et al., 2016). A few reactions were curated in the model, as described in Table S3. A biomass reaction (Table S1, see Methods) was added with a lower bound equal to the measured growth rate (Table S4). The non-growth associated ATP maintenance (NGAM) has been previously reported as 1.833 mmol gDW<sup>-1</sup> h<sup>-1</sup> (Kilburn et al., 1969), although results in our study were robust to variations in NGAM (Figure S2).

In the unconstrained input model, carbon-source exchanges are constrained to a maximum uptake of 10 mmol gDW<sup>-1</sup> h<sup>-1</sup> to avoid internal reaction bounds limiting the uptake of large polymeric carbohydrate molecules, which when catabolized lead to large fluxes in the model. Carbon-sources include all model metabolites with at least one carbon atom, except for CO<sub>2</sub> and HCO<sub>3</sub>. Other exchange reactions use the original flux bounds of the Recon 1 model (either 1000 or -1000 mmol gDW<sup>-1</sup> h<sup>-1</sup>). As no exometabolomics data are used to constrain the unconstrained model, it is the same for each of the four cell lines.

The constrained and semi-constrained models use exometabolomics data measured for the NCI-60 cell lines (Jain et al., 2012). To correct for mass spectrometer drift in the peak area quantification of the data, we used a nonlinear correction since the drift was nonlinear. Exchange reactions were constrained by using the maximum and minimum fluxes measured for the biological replicates of the corresponding cell lines. Bounds were expanded to include zero flux to ensure to not force uptake or secretion. For the constrained model quantitative values are used. For the semi-constrained model the directionality of the measured exchanges is qualitatively constrained by values of either -10, 0 or 10, based on the flux direction suggested by the exometabolomics data. Metabolite exchanges that were not in the data can only be excreted in the semi-constrained and constrained models, except for metabolites

that are not carbon sources, for which default bounds are used. Since the A375 cell line is not in the NCI-60 and no exometabolomics data are available, exchanges were constrained using data for all other melanoma cell lines in the NCI-60. Specifically, we constrained the model using the median of the forward fluxes and the median of the backward fluxes across all melanoma cell lines.

To ensure that the constrained and semi-constrained models can produce biomass, we reconsidered four exchange reactions in all of the cell types: histidine, methionine, saturated- and unsaturated octadecanoate exchange. These metabolites were not measured in the exometabolomic data, hence their uptake was constrained to zero. However, uptake of these metabolites is required for biomass production. For the semi-constrained models the maximum uptake is set to  $10 \text{ mmol gDW}^{-1} \text{ h}^{-1}$  for these metabolites, consistent with all other metabolites that can be taken up in the semi-constrained models. For the constrained models the maximum uptake rates for these metabolites are set to the minimum possible flux, based on a flux variance analysis (FVA) (Mahadevan and Schilling, 2003) in which biomass is constrained to have at least the flux it would have when uptakes of these metabolites were unbounded. The same is done for cysteine, which is not measured in the exometabolomic data but is assumed to be taken up by the cells (Gout et al., 1997). This resulted in constrained uptake rates comparable to other metabolites in the exometabolomics data.

All blocked reactions that are unable to carry flux above a certain threshold are removed. For the constrained models a threshold of  $1 \times 10^{-8}$  is chosen. For the unconstrained and semi-constrained models a threshold of  $1 \times 10^{-6}$  is chosen since metabolite uptakes were higher for these. A summary of the input models is given in Table S5. To verify that the results in this study were generalizable to other human metabolic networks, we also tested the main analyses in this study on Recon 2.2 (Swainston et al., 2016), which was published after this study had been completed. All analyses resulted in similar results based on Recon 1, as shown in Methods.

### RNA-Seq Data Processing

The mRNA-sequencing datasets (Bürkstümmer et al., 2013; Di Ruscio et al., 2013; Pawlikowski et al., 2013; Zhang et al., 2015) were downloaded, and Trimmomatic (Bolger et al., 2014) was used to trim low quality reads. The reads were aligned to the GRCh38 reference human genome using STAR (Dobin et al., 2013) (4 STAR parameters were set: '-outSAMstrandField intronMotif', '-outFilterType BySJout', '-outFilterIntronMotifs RemoveNoncanonicalUnannotated', '-outSAMtype BAM SortedByCoordinate', others are set as default), and then quantified using Cufflinks with all parameters set as defaults (Trapnell et al., 2011), using the unit of fragments per kilobase of exon per million fragments (FPKM) for all genes. Gene expression threshold cutoffs were determined from the data for each cell line (Table S6). The gene expression data were mapped to reactions using the GPRs, with OR logic using the maximum of the expression of all corresponding genes, and AND logic using the minimum of the expression of all the genes. Reactions without a GPR or where expression data is missing are not assigned a value.

### Processing of the Knockout Screen Data

Genome-scale CRISPR-Cas9 knockout screens (Shalem et al., 2014; Wang et al., 2014, 2015) were used to determine gene-essentiality in each cell line to validate the models. For each cell line, the mean  $\log_2$  sgRNA ratio (before vs. after screen) is calculated for each gene. The mean ratio is computed from the mean of all sgRNAs mapping to the same gene. For A375, K562 and KBM7, the ratios were calculated between days 3 and 14 post infection (Shalem et al., 2014; Wang et al., 2015). For HL60, the ratios compared 24 hr after infection and after twelve cell doublings (Wang et al., 2014). Gene identifiers are translated using bioDBnet 2.0 (Mudunuri et al., 2009). The numbers of genes in the data that could be mapped to genes in the model are shown in Table S7.

### Predictions of Gene-Essentiality

To predict gene-essentiality, the FBA algorithm from the COBRA Toolbox (Schellenberger et al., 2011) was used to optimize biomass production following the removal of each reaction in the cell line-specific models that would be affected by gene removal based on the GPRs. Using previously published criteria (Yang et al., 2014), a gene is essential when the maximum growth rate after knockout is less than 1% of the maximum growth rate before knockout. However, our results are qualitatively robust to changes in threshold choice for essentiality. A 1-tailed Wilcoxon rank sum test was used to test whether the  $\log_2$  sgRNA ratios were significantly lower for the genes that the model predicted to be essential. The p-value resulting from this test is used as an accuracy score. The contribution to the variance in p-values due to the different factors (constraint type, MEM and expression threshold) is calculated as follows. For each factor, the maximum Pearson correlation coefficient (R) of the p-values and categories is calculated across all possible orderings of the categories. The explained variance of each test reported is the  $R^2$ , scaled to percentage.

### Calculating the Functionality Score

Metabolic functionalities are the ability to synthesize individual metabolites of relevance to the cell line. As a proxy for all possible metabolic functionalities, we defined 56 different functionalities, which are 56 metabolites required for cancer growth. Prior to model extraction, the biomass reaction was removed and a sink reaction is added for each of the 56 metabolites to ensure they can be synthesized in the input model. All parameter sets were used in this analysis, and all MEMs were tested except for GIMME, which was not included because it includes the optimization of biomass, thus not allowing an unbiased assessment of its ability to perform the metabolic functions.

Following model extraction, all 56 functionalities were tested on each cell line-specific model as follows. First, the flux through the sink reaction for each functionality was maximized using FBA. If the sink can carry flux above the reaction activity threshold, the functionality is considered active. The reaction activity threshold is  $1 \times 10^{-8}$  for models extracted from a constrained input model and  $1 \times 10^{-6}$  for models extracted from unconstrained and semi-constrained input models.

The absolute number of active functionalities varies depending on model size. Therefore, a metric was developed to assess the efficacy of parameters and MEMs at predicting functionalities while controlling for model size. Specifically, the number of active functionalities was calculated for each model, compared to 1000 models of the same size, generated by randomly removing reactions from the input model. These random models are checked to ensure their stoichiometric consistency by also removing reactions that have been inactivated by the initial random removal. A quadratic relationship is then fitted between the number of reactions of each model and the number of functionalities they yield. The 99% confidence interval (non-simultaneous observation bounds) is calculated for the quadratic fits. Resulting is an upper bound for the 99% confidence interval for each unique input model. The score of a cell line-specific model is the distance from the 99% confidence interval at the same number of reactions (Figure S11). This is the number of functionalities the cell line-specific model has beyond the number exhibited by the top 1% of random models of the same size.

### Extraction of Cell Line-specific Models Using the MEMs

Two sets of models were extracted. The first set consisting of 288 models is used in the PCA, growth rate predictions and gene-essentiality analyses. For this set of models the biomass reaction is always given a lower bound equal to the in vitro growth rate of the corresponding cell before model extraction (Table S4). The second set consisting of 240 models is used for the metabolic functionality analysis. For these models, the biomass reaction is not given a constraint and will always be removed during model extraction.

Whenever a consistency check is performed during or after model extraction, fastCC (Vlassis et al., 2014) was used with a reaction activity threshold of  $1 \times 10^{-8}$  for the constrained model and  $1 \times 10^{-6}$  for the unconstrained and semi-constrained models. All MEMs are implemented in MATLAB and simulations are done using the COBRA Toolbox 2.0 (Schellenberger et al., 2011) in MATLAB 2013b. Gurobi5 is used as solver.

### Results from Recon1 Are Generalizable to Other Human Reconstructions

Recon 1 was used in this study because of its availability, quality, and because its size was more amenable to rapid model construction and analysis. However, more recent reconstructions, Recon 2 (Thiele et al., 2013) and Recon 2.2 (Swainston et al., 2016), and other updates (Quek et al., 2014) have been published and provide more extensive views of human metabolism. Thus, we tested if the results in our study with Recon 1 were generalizable to other human reconstructions. To do this we constructed models of the K562 cell line using Recon 2.2. Models were constructed using GIMME, FASTCORE, iMAT, INIT, and mCADRE. First, we found that, as seen using Recon 1, the gene expression threshold choice had the largest influence on the first principal component (Figure S12A), while the choice of constraint had its greatest contribution to the fourth principal component. However, when gene essentiality of the models was compared to data from the CRISPR-Cas9 loss of function screens, the MEM choice had the greatest influence on model accuracy (Figure S7). Furthermore, the pattern of optimal threshold and MEMs for gene essentiality predictions for Recon 2.2 (Figure S12B) is comparable with the results from Recon 1. Lastly, when models were constructed without the biomass function, the models were able to recapitulate most metabolic functions, but the few missing metabolic functions (Figure S12C) were comparable to those missing from models built with Recon 1 (Figure 4). Thus, the results seen with Recon 1 are generalizable to other human reconstructions.

### MILP-Based MEMs Have Multiple Solutions Performing Equivalently

Some MEMs, such as iMAT and MBA, utilize mixed integer linear programming (MILP), and as a result, the MEMs can yield multiple solutions for a model extraction that would be equally “fit” to the input data. We tested here how different the equivalently optimal models are from each other, and demonstrated that they exhibit similar levels of accuracy. Specifically, we generated equivalent optimal models of the A375 cell line constructed using iMAT or MBA (with the p25 threshold) by running the algorithms ten different times, using different random seeds to start the algorithm. We found that the ability to predict gene essentiality did not drastically change (Figure S3). Indeed, for example, the results from the analyses in which we predicted gene essentiality for the 10 different optimal MBA models represent yielded similar results. Furthermore, while the models show some differences in reaction content, we found them to vary far less in reaction content among the alternative optimal models, compared to models generated with different MEMs (Figure S4).

### Minor Changes to the Biomass Composition Does Not Significantly Influence Gene Essentiality Results

The biomass function was built from previously published studies (Table S1). However, we carefully curated it to qualitatively cover many of the metabolic needs of most, if not all cancer cell lines. Thus, it accounts for the components that are necessary for an immortalized cell line to grow. This includes the amino acids, nucleotides, sugars, energy equivalents, and essential small metabolites (polyamines, glutathione, q10, paps, carnitine, tetrahydrobiopterin, etc.). The quantitative values should be near the actual values for the cell lines, but they are estimates based on published sources of cancer cell lines and a few others immortalized mammalian cell lines (Altamirano et al., 2001; Bonarius et al., 1996; Sheikh et al., 2005). While the values will vary across cell lines, we note that the quantitative values in a biomass function only rarely affect gene essentiality predictions (only if substrate uptake rates end up conflicting, which would not accurately reflect the biology since actual cell lines would merely reduce uptake of any conflicting metabolite). Indeed, a recent study demonstrated that predictions of growth rates and metabolic flux predictions are largely robust to changes in the quantitative values of a biomass function (Yuan et al., 2016). To test the validity of this statement in the context of our study, we used mCADRE to generate 10 additional models for the A375 cell line. For each of these models, all biomass coefficients were

randomly varied by 20%. We do not see any difference in the accuracy results (i.e., the accuracy scores for gene essentiality predictions were the same for all 10 models, and predicted growth rates varied by <6%). This analysis demonstrates that modest changes in the biomass coefficients do not significantly impact the construction of models, nor the accuracy of gene essentiality predictions using these models. We further tested if the results were also robust to changes in the composition to the biomass function. Specifically, while a thorough characterization was made to include even low abundance essential vitamins in the biomass function, it is possible that the biomass function could be missing components. In this situation, the models could erroneously miss some essential genes. To test if this could potentially impact the claims of our study, we have performed a supplementary analysis in which we built 10 more models of the A375 cell line using mCADRE after randomly adding a non-biomass metabolite to the biomass function. After adding these metabolites, our results were qualitatively the same (Figure S1), and well within the range seen for the models built using the standard biomass function used for this study (Figure S7).

### Extracted Models Do Not Inherently Predict Growth Rates

Constraint-based modeling is particularly valuable in its ability to successfully simulate cellular functions and phenotypes, based on an organism's metabolic network. Thus, to assess the ability for the models to predict phenotypes, we tested their ability to predict growth rates. Cell line-specific models that are extracted from constrained input models are directly used to predict growth rate. Cell line-specific models that are extracted from a semi-constrained or unconstrained input model were constrained by the measured uptake rates for all exchange reactions that remained after model extraction. Prior to model extraction, the experimentally measured growth rate (see Table S4) was added as a lower bound on the biomass reaction. This constraint is removed since models might not be able to achieve this growth rate after the exchange reaction constraints were added. The growth rate is then predicted by maximizing the biomass reaction using FBA. We found that in nearly all cases, the unconstrained and semi-constrained models failed to recapitulate the experimentally measured growth rate of the cell. Out of all cell line-specific models extracted from unconstrained and semi-constrained input models, only 7% could achieve a biomass production above 50% of the experimentally measured growth rate. This failure results because when starting with the non-quantitative uptake and secretion rates, the MEMs are not constrained to keep the pathways required by the exometabolomics data. Thus, important cell pathways are eliminated since the required experimentally measured growth rates can easily be met with unrealistic uptake rates of specific metabolites that can be used to synthesize many other biomass metabolites. This occurs since many pathways and uptakes are deemed redundant during extraction and are therefore removed. Then, when measured uptake rates are added, the cell line-specific models are lacking pathways and cannot produce sufficient biomass. Thus, cell-line specific models can only accurately recapitulate growth rates if uptake and secretion rates from exometabolomic data are set prior to model extraction (i.e., in the constrained input model) and the biomass reaction itself is given a lower bound as well.

## QUANTIFICATION AND STATISTICAL ANALYSIS

### Principal Component Analysis

A binary matrix is constructed in which each row represents one of the 72 extracted models and each column represents a variable: a reaction being present (1) or absent (0) in a model for the model content PCA. Reactions in all or no models were removed from the matrix. Similarly for the metabolic functionality PCA, the matrix had each row as an extracted model and each column a variable: a functionality being present (1) or absent (0) in the model. For the PCAs, the matrix was centered to have zero mean within each row. A PCA analysis on this matrix was conducted. The variance explained by the different factors (constraint type, MEM and expression threshold) within each of the principal components is calculated as follows. Within one factor, the maximum Pearson correlation coefficient (R) of the component scores and categories is calculated across all possible orderings of the categories. Reported is the R<sup>2</sup> scaled to percentages.

### DATA AND SOFTWARE AVAILABILITY

The mRNA-sequencing datasets were acquired from previous publications (Bürkstümmer et al., 2013; Di Ruscio et al., 2013; Pawlikowski et al., 2013; Zhang et al., 2015) and genome-scale CRISPR-Cas9 knockout screens were obtained from (Shalem et al., 2014; Wang et al., 2014, 2015). Matlab code for running extraction methods and performing analysis are provided in Data S1 (see also [https://github.com/LewisLabUCSD/Context\\_Specific\\_Models\\_from\\_GeMS](https://github.com/LewisLabUCSD/Context_Specific_Models_from_GeMS)).